Effects of Wall Slip on Convective Heat Transfers of Giesekus Fluid in Microannulus

Mehdi Moayed Mohseni, Gilles Tissot, Michael Badawi

Effects of Wall Slip on Convective Heat Transfers of Giesekus Fluid in Microannulus

Mehdi Moayed Mohseni
Laboratoire de Physique et Chimie Théoriques (LPCT, UMR CNRS UL 7019), Université de Lorraine, Rue Victor Demange, Saint-Avold 57500, France

Gilles Tissot
INRIA Rennes Bretagne Atlantique, IRMAR—UMR CNRS 6625, Avenue Ge□ne□ral Leclerc, Rennes 35042, France

Michael Badawi
Laboratoire de Physique et Chimie Théoriques (LPCT, UMR CNRS UL 7019), Université de Lorraine, Rue Victor Demange, Saint-Avold 57500, France

Convective heat transfer and effect of nonlinear wall slip are studied analytically in con-centric microannulus for viscoelastic fluids obeying the Giesekus constitutive equation. Laminar, thermally, and hydrodynamically fully developed flow is considered. A nonlinear Navier model with nonzero slip critical shear stress is employed for the slip equation at both walls. Critical shear stress will cause three slip flow regimes: no slip condition, slip only at the inner wall, and slip at both walls. Thermal boundary conditions are assumed to be peripherally and axially constant fluxes at the walls. Governing equations are solved to obtain temperature profiles and Nusselt number and effects of slip parame-ters, elasticity, and Brinkman number are discussed. Two regimes are compared when slip occurs at both walls or only at the inner wall. The results indicate that by increasing slip effect and elasticity, heat transfer between wall and fluid is enhanced, but it decreases by increasing Brinkman number. In the case where the heat flux is dominant in the outer wall, the inner wall Nusselt curve shows a singularity for a critical Brinkman number because at this Brinkman number the bulk temperature will be equal to the wall temperature.

Keywords: microannulus, Giesekus constitutive equation, slip, elasticity, viscous dissipation

1 Introduction

Microfluidics refers to the technology of the fluid systems when the range of flow is between microliters and picoliters inside a microchannel [1]. Due to small scales, the Reynolds number for microfluidics flow is low; therefore, the flow regime of these systems will be laminar [2]. Several microfluidics devices (micropumps, microvalves, microreactors, mixers, measurement devices and….) get together on a chip is fabricated a Lab-on-a-chip. Lab-on-a-chip is a subset of microelectromechanical systems devices which sometimes called micrototal analysis systems [3]. The use of microfluidic devices has some advantages which can be mentioned in the following: minimizing material and sample consumption, reduction in power budget, faster devices, and using for applications which demand small volume of fluid. Microfluidics systems have a wide range of applications such as medical science, drug delivery, DNA sequencing, bio-microelectromechanical systems, point-of-care testing, analytical chemistry, and biotechnology [4,5]. In most of these systems, heat transfer between the fluid and its environment is essential. Therefore, understanding and predicting heat transfers are of particular interest for the manufacturing and operation of these systems. In most cases, the fluids that flow in microdevices have non-Newtonian rheological behavior, for example, in biomedical systems or in the bioreactors [1]. Empirical evidences [6] indicate that the wall slip may occur in many complex fluids such as suspensions, emulsions, polymer melts and solutions due to adhesive failure, cohesive failure or formation of a low viscosity layer of solvent at wall. The three slip mechanisms are shown in Fig. 1.

Since these phenomena rely on Nano/microscale mechanisms, most of the mathematical models used for expressing it are strongly empirical. We have chosen in this study to employ the nonlinear Navier slip law.

This model consists in a power law relationship between slip velocity and shear stress at the wall as follows, which has been used in many studies [7–12]:

$$\mathbf{u}_w = \left(\frac{|\boldsymbol{\tau}_w|}{\beta}\right)^{\frac{1}{s}} \tag{1}$$

where s is the power law index and β is slip coefficient which depends on the temperature, the normal stress, the molecular parameters, and properties of the fluid/wall interface [6]. The no slip boundary condition and plug flow are recovered when β tends to infinity and zero, respectively. Also, surveys indicate that slip occurs only when the wall shear stress (τ_{rzw}) exceeds a critical value (τ_c); therefore, the nonlinear Navier slip model is employed in the following form [7]:

$$\begin{cases} \mathbf{u}_w = 0 & |\boldsymbol{\tau}_{rz\,w}| \le \boldsymbol{\tau}_c \\ \mathbf{u}_w = \left(\dfrac{|\boldsymbol{\tau}_{rz\,w}| - \boldsymbol{\tau}_c}{\beta}\right)^{\frac{1}{s}} & |\boldsymbol{\tau}_{rz\,w}| > \boldsymbol{\tau}_c \end{cases} \tag{2}$$

Extensive literature exists regarding the effect of slip condition for Newtonian and non-Newtonian fluids [7–19] but heat transfers in the presence of slip at walls is less studied which can be mentioned in the following.

Numerical approaches have been proposed to investigate circular and rectangular microchannels [20,21] for Ostwald–de Waele power law fluid. The slip velocity is defined as a coefficient of mean velocity of fluid in these studies.

Shjaeian and Kosar [22] studied both convective heat transfer and entropy generation of microfluidic flow for Newtonian and non-Newtonian fluids between parallel plates with linear Navier slip velocity boundary condition and using analytical method. The first and second laws of thermodynamics [22] were investigated for power law fluids by Anand [23] in microchannel using nonlinear Navier, Hatzikiriakos, and asymptotic slip laws. Kiyasatfar [24] carried out a similar research inside both parallel plates and circular microchannels with only nonlinear Navier slip law. For

[1]Corresponding author.

viscoelastic fluid, an analytical solution was presented by Norouzi and Rezaie with Phan-Thien–Tanner model and nonlinear Navier slip law inside microtubes. Finally, Mohseni et al. [25] proposed an analytical approach for Giesekus viscoelastic fluids with nonlinear Navier models in pipes.

As mentioned in the literature, all of the studies about the influence of slip phenomena on heat transfer are limited to the single wall geometry such as pipes and circular microchannels or symmetric double wall geometry such as parallel plates. In both of them, there is only one shear stress at the wall; therefore, there will be one slip regime. But in the annulus, there are two asymmetric walls with two different wall shear stresses which lead to two slip regimes. The investigation of heat transfer in this kind of circumstances is missing in literature up to now. Indeed, the main aim of this study is to present the analytical solution of forced convection heat transfer for laminar, steady-state and fully developed flow in microannulus for nonlinear viscoelastic fluid obeying Giesekus model accounting slip condition at walls. The slip laws at both walls employed are nonlinear Navier with nonzero slip critical shear stress.

2 Governing Equations

The problem is considered to be steady, laminar, and both thermally and hydrodynamically fully developed flow in the microannulus-axis direction (see Fig. 2). Axial heat conduction is neglected compared to the heat transfer in the radial direction from the order of magnitude analysis [26]. The effect of viscous dissipation is included because most of viscoelastic fluids such as polymeric melts and solutions have high viscosity.

We assume that the temperature variations are small enough to consider that the thermophysical properties of the fluid are constant [27–29]. R_i and R_o are inner and outer cylinder radiuses, respectively. The annular gap is defined as $\delta = R_o - R_i$.

The continuity, momentum, and Giesekus constitutive equations (without retardation time) are

$$\nabla \cdot \mathbf{u} = 0 \tag{3a}$$

$$\rho \frac{D\mathbf{u}}{Dt} + \nabla P = \nabla \cdot \boldsymbol{\tau} \tag{3b}$$

$$\boldsymbol{\tau} + \frac{\alpha\lambda}{\eta}(\boldsymbol{\tau}\cdot\boldsymbol{\tau}) + \lambda\frac{\vartheta\boldsymbol{\tau}}{\vartheta t} = \eta\dot{\boldsymbol{\gamma}} \tag{3c}$$

where u is the velocity field, P the pressure, $\boldsymbol{\tau}$ the stress tensor

$$\dot{\boldsymbol{\gamma}} = [\nabla\mathbf{u} + (\nabla\mathbf{u})^T] \tag{4}$$

$$\frac{\vartheta\boldsymbol{\tau}}{\vartheta t} = \frac{D\boldsymbol{\tau}}{Dt} - \left[\boldsymbol{\tau}\cdot\nabla\mathbf{u} + (\nabla\mathbf{u})^T\cdot\boldsymbol{\tau}\right] \tag{5}$$

$$\frac{D\boldsymbol{\tau}}{Dt} = \frac{\partial\boldsymbol{\tau}}{\partial t} + (\mathbf{u}\cdot\nabla)\boldsymbol{\tau} \tag{6}$$

Giesekus constitutive Eq. (3c) is a nonlinear dynamical three parameter model of the stress tensor based on molecular phenomenology.

η is the zero shear viscosity, λ is the zero shear relaxation time, and α is the mobility factor, lying in the range $0 \le \alpha \le 1$ [30,31]. The relaxation time is the time needed for the stresses to relax after the fluid motion has stopped. It is a characteristic of viscoelastic fluids [32]. Rigorously, the model parameters are function of shear rate, but they approach to a constant value at very low shear rate: so-called zero shear model parameters. We can note that the nonlinear term containing α in Eq. (3c) is attributed to anisotropy. It permits to take into account anisotropic Brownian motion or anisotropic hydrodynamic drag on the constituent polymer molecules [28].

The energy equation with considering assumptions is represented as follows:

$$\rho\, c_p u\frac{\partial T}{\partial z} = \frac{k}{r}\frac{\partial}{\partial r}\left(r\frac{\partial T}{\partial r}\right) + \Phi \tag{7}$$

where k, ρ, and c_p are thermal conductivity, density, and specific heat capacity of the fluid, respectively. T is the temperature and Φ is the dissipation function which includes only the shear stress and the shear rate for this flow, and described as follows:

$$\Phi = \tau_{rz}\frac{\partial \mathbf{u}}{\partial r} \tag{8}$$

The thermal boundary conditions are peripherally and axially constant heat fluxes at both walls as follows:

$$r = R_i - k\frac{\partial T}{\partial r} = q_i \tag{9a}$$

$$r = R_o\, k\frac{\partial T}{\partial r} = q_o \tag{9b}$$

Axially, we consider [33]

$$\frac{\partial}{\partial z}\left(\frac{T_w - T}{T_w - T_b}\right) = 0 \tag{10}$$

where T_w and T_b represent the wall and bulk temperatures, respectively. Bulk temperature is defined as follows:

$$T_b = \frac{\int_{R_i}^{R_o} 2\pi\, r\mathbf{u}T dr}{\int_{R_i}^{R_o} 2\pi\, r\mathbf{u} dr} \tag{11}$$

For the imposed heat flux case, Eq. (10) reduces to

$$\frac{\partial T}{\partial z} = \frac{\partial T_w}{\partial z} = \frac{\partial T_b}{\partial z} \tag{12}$$

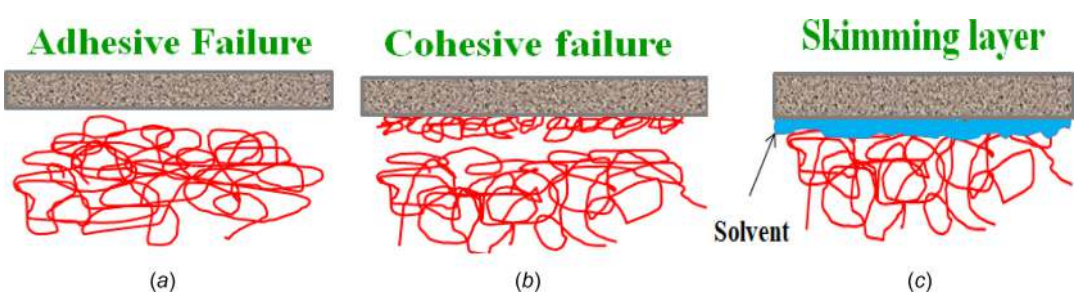

Fig. 1 Schematic diagram of slip mechanism: (*a*) adhesive failure, (*b*) cohesive failure, and (*c*) skimming layer formation

This value, fixing the thermal axial dependency, can be determined by applying energy balance over an infinitesimal slice of fluid of thickness, dz in the axial direction. The following equation is obtained for axial gradient of fluid bulk temperature

$$\frac{\partial T_b}{\partial z} = \frac{2}{\rho U c_p \left(R_o^2 - R_i^2\right)} \left[q_i R_i + q_o R_o + \int_{R_i}^{R_o} r \tau_{zr} \frac{\partial \mathbf{u}_z}{\partial r} dr \right] \tag{13}$$

Let us now turn out the problem dimensionless by defining the following variables:

$$\overline{r} = \frac{r}{\delta}, \quad \overline{z} = \frac{z}{\delta}, \quad \overline{u} = \frac{\mathbf{u}}{U}, \quad \overline{\gamma} = \frac{\boldsymbol{\gamma}}{U/\delta}, \quad \overline{\tau} = \frac{\boldsymbol{\tau}}{\eta U/\delta},$$
$$\psi = \frac{\delta^2}{\eta U} \left(\frac{dp}{dz}\right), \quad \Theta = \frac{k(T - T_b)}{2\delta q^{\circ}}$$

where p, u, and γ are the pressure, velocity, and shear rate, respectively. Also, ψ is the dimensionless group for pressure gradient and U is the average velocity over a cross section of the microannulus, which is described as follows:

$$U = \frac{\int_{R_i}^{R_o} 2\pi r \, \mathbf{u} \, dr}{\int_{R_i}^{R_o} 2\pi r \, dr} \tag{14}$$

Θ is dimensionless local temperature. q° is the perimeter average wall heat flux and is defined as follows:

$$q^{\circ} = \frac{q_i R_i + q_o R_o}{R_i + R_o} = \frac{R_i + \phi R_o}{R_i + R_o} \tag{15}$$

where ϕ is the ratio of outer and inner wall heat fluxes, $\phi = q_o/q_i$.

We define as well the Brinkman number Br, which is a measure of importance of the viscous dissipation term

$$Br = \frac{\eta U^2}{2\delta q^{\circ}} \tag{16}$$

By combining Eqs. (7), (12), and (13) and using dimensionless terms, the dimensionless differential energy equation is obtained

$$\frac{1}{\overline{r}} \frac{\partial}{\partial \overline{r}} \left(\overline{r} \frac{\partial \Theta}{\partial \overline{r}} \right) = X \, \overline{\mathbf{u}} - Br \overline{\Phi} \tag{17}$$

where

$$X = \frac{1 + 2Br \int_{\overline{R}_i}^{\overline{R}_o} \overline{r} \, \overline{\tau} \frac{\partial \overline{\mathbf{u}}}{\partial \overline{r}} d\overline{r}}{\left(\overline{R}_o^2 - \overline{R}_i^2\right)} \tag{18a}$$

$$\overline{\Phi} = \overline{\tau} \frac{\partial \overline{\mathbf{u}}}{\partial \overline{r}} \tag{18b}$$

Details regarding X are presented in the Appendix. Moreover, dimensionless thermal boundary conditions are

$$\frac{\partial \Theta}{\partial \overline{r}} = -\frac{1}{2} \frac{\overline{R}_i + \overline{R}_o}{\overline{R}_i + \phi \overline{R}_o} \quad \overline{r} = \overline{R}_i \tag{19a}$$

$$\frac{\partial \Theta}{\partial \overline{r}} = \frac{\phi}{2} \frac{\overline{R}_i + \overline{R}_o}{\overline{R}_i + \phi \overline{R}_o} \quad \overline{r} = \overline{R}_o \tag{19b}$$

Also, the dimensionless form of the slip boundary conditions is as follows:

$$\overline{r} = \overline{R}_i \begin{cases} \overline{\mathbf{u}}_{wi} = 0 & \overline{\tau}_{rz}\left(\overline{R}_i\right) \le B_c \\ \overline{\mathbf{u}}_{wi} = \left(\dfrac{\overline{\tau}_{rz}\left(\overline{R}_i\right) - B_c}{B} \right)^{\frac{1}{s}} & \overline{\tau}_{rz}\left(\overline{R}_i\right) > B_c \end{cases} \tag{20a}$$

$$\overline{r} = \overline{R}_o \begin{cases} \overline{\mathbf{u}}_{wo} = 0 & -\overline{\tau}_{rz}\left(\overline{R}_o\right) \le B_c \\ \overline{\mathbf{u}}_{wo} = \left(\dfrac{-\overline{\tau}_{rz}\left(\overline{R}_o\right) - B_c}{B} \right)^{\frac{1}{s}} & -\overline{\tau}_{rz}\left(\overline{R}_o\right) > B_c \end{cases} \tag{20b}$$

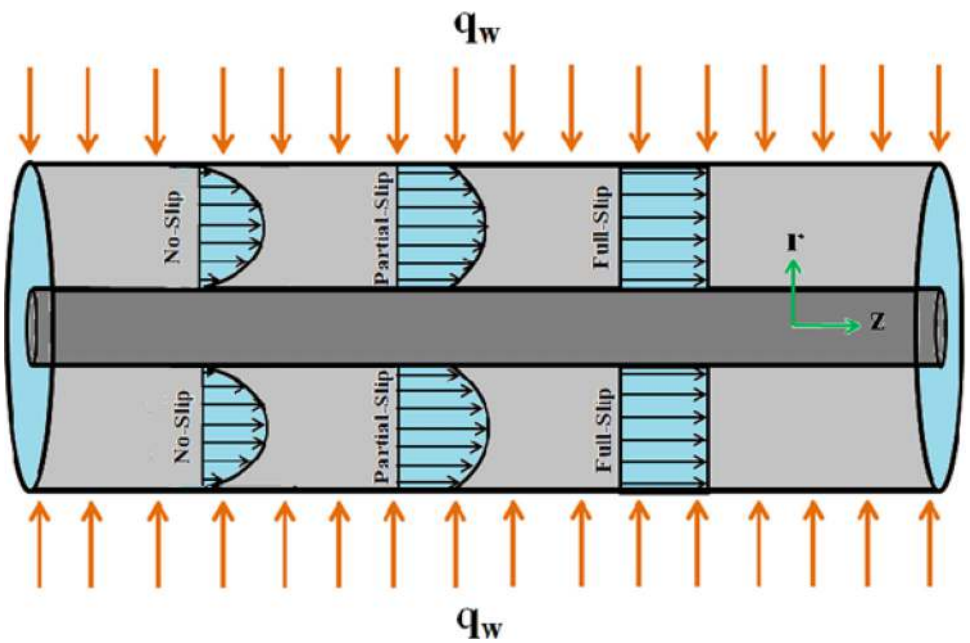

Fig. 2 Schematic diagram of the annulus and its slip and thermal boundary conditions

B and B_c are dimensionless slip number and dimensionless slip critical shear stress number, respectively, and are defined as follows:

$$B = \frac{\beta\delta\, U^{s-1}}{\eta} \qquad B_c = \frac{\tau_c \delta}{\eta U}$$

3 Analytical Solution

In this study, we assume that the temperature variations are small enough such that the thermophysical proprieties remain constant. This allows a decoupling between thermal and hydrodynamic solution. Once the velocity profile is known, the temperature profile can be deduced.

3.1 Hydrodynamic Solution. The shear stress equation for annular geometry is derived from Eq. (3*b*) after integration in the z direction as follows:

$$\overline{\tau}_{rz} = \frac{\psi \overline{R}_m}{2} \quad \frac{\overline{r}}{\overline{R}_m} - \frac{\overline{R}_m}{\overline{r}}\Bigg) \tag{21}$$

$\overline{R}_m$ refers to the radius where the $\overline{\tau}_{rz} = 0$.

Following Yoo and Choi [34], we obtain the shear rate equation

$$\overline{\gamma}_{rz} = \frac{\mathrm{d}\overline{\mathbf{u}}}{\mathrm{d}\overline{\mathrm{r}}} = 2\alpha\overline{\tau}_{rz}\frac{1 \pm (2\alpha-1)\sqrt{1-4\alpha^2 De^2 \overline{\tau}_{rz}^2}}{\left(2\alpha - 1 \pm \sqrt{1-4\alpha^2 De^2\overline{\tau}_{rz}^2}\right)^2} \tag{22}$$

where De is the Deborah number, defined as ($De = \lambda U/R$) and related to the level of fluid elasticity.

Schleiniger and Weinacht [35], using linear stability analysis and Yoo and Choi [34] by employing thermodynamic considerations, have indicated that for the case of no-solvent viscosity of Giesekus model, only the positive sign will result in a physically realistic solution. Therefore, the positive sign will be considered for continuing of solution. In the following, we will consider an approximate solution approach [7,36,37] for deriving the velocity profile in order to obtain the analytic expression for temperature profile. Indeed, it is not possible when the exact velocity profile is coupled in energy equation. To do so, the term $\sqrt{1-4\alpha^2 De^2\overline{\tau}_{rz}^2}$ in Eq. (22) is expressed by a power series using the binominal expansion as follows:

$$\sqrt{1-4\alpha^2 De^2\overline{\tau}_{rz}^2} \cong 1 - 2\alpha^2 De^2\overline{\tau}_{rz}^2 \tag{23}$$

where all terms of higher order have been neglected compared to the leading term in the approximation which is valid for small values of $4\alpha^2 De^2\overline{\tau}_{rz}^2$. Truncation error is less than 6% when $4\alpha^2 De^2\overline{\tau}_{rz}^2$ is less than 1/2. The Truncation error is obtained from percentage error formula as follows:

$$\begin{aligned}\mathrm{PE}\% &= \frac{|\text{approximate value} - \text{exact value}|}{|\text{exact value}|} \\ &= \frac{|1 - 2\alpha^2 De^2\overline{\tau}_{rz}^2 - \sqrt{1-4\alpha^2 De^2\overline{\tau}_{rz}^2}|}{\sqrt{1-4\alpha^2 De^2\overline{\tau}_{rz}^2}} \times 100\% \end{aligned} \tag{24}$$

Since the slip effect reduces $|\overline{\tau}_{rz}|$ which causes $4\alpha^2 De^2\overline{\tau}_{rz}^2$ to decrease hence, accuracy of approximation will be higher than 94% for the wide range of α and De. Also, by moving away from the walls of annulus, $|\overline{\tau}_{rz}|$ and subsequently $4\alpha^2 De^2\overline{\tau}_{rz}^2$ decrease which causes to increase accuracy [7].

By substituting Eq. (23) in Eq. (22) and integrating in the radial direction, dimensionless velocity profile can be obtained as follows:

$$\int_{\overline{R}_i \bar{r}} \overline{\gamma}_{\mathrm{rz}} d\,\bar{r} = \overline{V}|_{\overline{R}_i}^{\bar{r}} \tag{25}$$

Then after integrating from Eq. (25), the velocity profile can be obtained as follows:

$$\overline{\mathbf{u}} = \overline{V}|_{\overline{R}_i \bar{r}} + \overline{u}_{wi} = \overline{V}(\bar{r}\ ) - \overline{V}(\overline{R}_i\,) + \overline{u}_{wi} \tag{26}$$

The first term of right-hand side of Eq. (26) is defined as follows:

$$\overline{V}\,(\bar{r}) = -\frac{\psi}{2P_1}\left(\overline{V}_1\,(\bar{r}) + \overline{V}_2\,(\bar{r}) + \overline{V}_3\,(\bar{r})\right) \tag{27a}$$

$$\overline{V}_1 = \frac{4(\alpha-1)\left[P_1\overline{R}_m^4 - (1+3P_2)\,\bar{r}^2\right]}{P_2\left[P_1\left(\overline{R}_m^4 + \bar{r}^4\right) - 2(1+P_2)\,\bar{r}^2\right]} \tag{27b}$$

$$\overline{V}_2 = \frac{P_3 + (2\alpha-1)P_2\sqrt{P_2}}{P_2\sqrt{P_2}}\ln\left[P_1\left(\bar{r}^2 - \overline{R}_m^2\right) + 2\left(\sqrt{P_2}-1\right)\right] \tag{27c}$$

$$\overline{V}_3 = \frac{(2\alpha-1)P_2\sqrt{P_2} - P_3}{P_2\sqrt{P_2}}\ln\left[P_1\left(\bar{r}^2 - \overline{R}_m^2\right) - 2\left(\sqrt{P_2}+1\right)\right] \tag{27d}$$

Expressions of P_1, P_2 are reported in the Appendix.

The second term, i.e., $\overline{V}(\overline{R}_i\,)$, is a constant value and is derived by substituting by $\overline{R}_i$ in Eq. (27), and the third term is the slip velocity at the inner wall and it is equal to

$$\overline{u}_{wi} = \left(\frac{\psi\overline{R}_m\left(\overline{R}_i/\overline{R}_m - \overline{R}_m/\overline{R}_i\right) - 2B_c}{2B}\right)^{\frac{1}{s}} \tag{28}$$

ψ and $\overline{R}_m$ are two unknown parameters in the velocity profile. To determine them, two independent equations are required.

One of these two equations is the velocity at the outer wall

$$\overline{V}|_{\overline{R}_i}^{\overline{R}_o} = \overline{\mathbf{u}}_{wo} - \overline{\mathbf{u}}_{wi} \tag{29a}$$

where

$$\overline{u}_{wo} = \left(\frac{\psi\overline{R}_m\left(\overline{R}_o/\overline{R}_m - \overline{R}_m/\overline{R}_o\right) - 2B_c}{2B}\right)^{\frac{1}{s}} \tag{29b}$$

The second independent equation is obtained prescribing the mass flux, i.e., using the dimensionless average velocity definition.

Dimensionless form of Eq. (14) is

$$\int_{\overline{R}_i}^{\overline{R}_o} \bar{r}\,\overline{\mathbf{u}}\,d\,\bar{r} = \frac{\overline{R}_o^2 - \overline{R}_i^2}{2} \tag{30}$$

After substituting the velocity equation in Eq. (30) and integrating the second equation will derive as follows:

$$\frac{\psi}{2P_1^2P_2}\,(U_1 + U_2 + U_3 + U_4)|_{\overline{R}_i}^{\overline{R}_o} = \overline{R}_o^2 - \overline{R}_i^2 \tag{31a}$$

$$\begin{aligned} U_1 = \frac{2(1-\alpha)}{\sqrt{P_5}} \quad & P_5 \arctan\left[\frac{2P_1\,(\bar{r})^2 - 2(1+P_2)}{\sqrt{P_5}}\right] \\ & -(1+3P_2)\ln\left[P_1\left((\bar{r})^4 + \overline{R}_m^4\right) - 2(1+P_2)\,(\bar{r})^2\right]\Bigg) \end{aligned} \tag{31b}$$

$$U_2 = -\sqrt{P_2^{-1}}\left(P_3 + (2\alpha-1)P_2\sqrt{P_2}\right)\left(-P_1\,(\overline{r})^2 + (P_6 + P_1(\overline{r})^2)\ln\left[P_6 + P_1(\overline{r})^2\right]\right) \tag{31c}$$

$$U_3 = \sqrt{P_2^{-1}}(-P_3 + (2\alpha-1)P_2\sqrt{P_2}) \times (P_7 - P_1(\overline{r})^2)\,(\ln\left[P_1(\overline{r})^2 - P_7\right] - 1\,) \tag{31d}$$

$$U_4 = (\overline{V}(\overline{R}_i) + \overline{\mathbf{u}}_{wi})\,(\overline{r})^2/2 \tag{31e}$$

Expressions of P_3 to P_7 are reported in the Appendix.

3.2 Thermal Solution. Once the velocity profile is available, we can determine the dimensionless temperature profile (Θ). It can be obtained by integration of Eq. (17)

$$\Theta = XU^* - Br\Phi^* + C_1\ln(\overline{r}\,) + C_2 \tag{32}$$

$$U^* = \int\frac{1}{\overline{r}}\int\overline{\mathbf{u}}\,\overline{r}\,d\overline{r}\,d\overline{r} \tag{33a}$$

$$\Phi^* = \int\frac{1}{\overline{r}}\int\overline{\Phi}\,\overline{r}\,d\overline{r}\,d\overline{r}\cdot \tag{33b}$$

Expressions of $\overline{U}$ and $\overline{\Phi}$ are presented in the Appendix.

Since both boundary conditions are of second type, Θ is defined up to a constant and C_2 cannot be determined directly. Hence, C_2 is eliminated from Eq. (32) by subtracting dimensionless wall temperatures (Θ_i and Θ_o) from dimensionless temperature profile (Θ)shown as follows:

$$\Theta - \Theta_i = X\,\left(U^* - U^*|_{\overline{R}_i}\right) - Br\left(\Phi^* - \Phi^*|_{\overline{R}_i}\right) + C_1\ln\left(\frac{\overline{r}}{\overline{R}_i}\right) \tag{34a}$$

$$\Theta - \Theta_o = X\,\left(U^* - U^*|_{\overline{R}_o}\right) - Br\left(\Phi^* - \Phi^*|_{\overline{R}_o}\right) + C_1\ln\left(\frac{\overline{r}}{\overline{R}_o}\right) \tag{34b}$$

C_1 can be obtained by injecting the boundary conditions Eq. (19a) or (19b) as follows:

$$C_1 = \overline{R}_i\left[Br\frac{d\Phi^*}{d\,\overline{r}}|_{\overline{r}=\overline{R}_i} - X\frac{dU^*}{d\,\overline{r}}|_{\overline{r}=\overline{R}_i} - \frac{1}{2}\frac{\overline{R}_i + \overline{R}_o}{\overline{R}_i + \varphi\,\overline{R}_o}\right] \tag{35a}$$

or equivalently

$$C_1 = \overline{R}_o\left[Br\frac{d\Phi^*}{d\,\overline{r}}|_{\overline{r}=\overline{R}_o} - X\frac{dU^*}{d\,\overline{r}}|_{\overline{r}=\overline{R}_o} - \frac{\varphi}{2}\frac{\overline{R}_i + \overline{R}_o}{\overline{R}_i + \varphi\,\overline{R}_o}\right] \tag{35b}$$

By substitution of temperature (T) from dimensionless local temperature expression into the bulk temperature equation and after simplifications, the following expressions for dimensionless wall temperatures are obtained:

$$\Theta_i = \frac{2}{\overline{R}_o{}^2 - \overline{R}_i{}^2}\int_{\overline{R}_i}^{\overline{R}_o}\overline{r}\,\overline{\mathbf{u}}(\Theta_i - \Theta)\,d\,\overline{r} \tag{36a}$$

$$\Theta_o = \frac{2}{\overline{R}_o{}^2 - \overline{R}_i{}^2}\int_{\overline{R}_i}^{\overline{R}_o}\overline{r}\,\overline{\mathbf{u}}(\Theta_o - \Theta)\,d\,\overline{r} \tag{36b}$$

After numerical integration of Eqs. (36a) and (36b), the convective heat transfer from walls to the fluid is quantified by the Nusselt number at inner (Nu_i) and outer (Nu_o) walls. Based on the hydraulic diameter ($D_H = 2\delta$), the Nusselt number is defined as ($\mathrm{Nu} = 2\delta\,h/k$). The heat transfer coefficient (h) at the walls is obtained from ($q_w = h(T_w - T_b)$). By using dimensionless temperature definition, the Nusselt number becomes ($\mathrm{Nu} = q_w/q^{\circ}\Theta_w$) and after substituting q° from Eq. (15), the following expression is obtained for inner and outer Nusselt numbers:

$$\mathrm{Nu}_i = \frac{\overline{R}_i + \overline{R}_o}{\overline{R}_i + \varphi\,\overline{R}_o}\frac{1}{\Theta_i} \tag{37a}$$

$$\mathrm{Nu}_o = \frac{\varphi\left(\overline{R}_i + \overline{R}_o\right)}{\overline{R}_i + \varphi\,\overline{R}_o}\frac{1}{\Theta_o} \tag{37b}$$

4 Results and Discussion

Three different values for the ratio between outer and inner wall heat flux (φ) are chosen for analysis which corresponds to the following situations:

$\varphi = 0.001$, the inner wall heat flux is very large compared to the outer wall heat flux; thus, fluid thermal behavior is similar to the one of an insulated outer wall.
$\varphi = 1000$, the heat flux at outer wall is much higher than the inner wall heat flux and the fluid thermal behavior is similar to that of an insulated inner wall.
$\varphi = 1$, the heat fluxes at both walls have a similar importance.

Since $|\tau_{wi}| > |\tau_{wo}|$ and according to Eqs. (20a) and (20b), slip first occurs at the inner wall therefore there are two slip flow regimes, slip only at the inner wall and slip at both walls which are detected by B_c with the following process. First, we assume the no slip boundary conditions are ruling at both walls and then the shear stress at inner wall is calculated and compare between the values of $|\tau_{wi}|$ and B_c. If $|\tau_{wi}| < B_c$, the no slip boundary conditions at both walls have been a correct assumption but if $|\tau_{wi}| > B_c$, the slip certainly will occur at the inner wall or at both walls. It should be noted that the slip condition affects the value of ψ; thus, the shear stress at walls will change and should be calculated again. Since the slip first occurs at the inner wall, in this step just the slip velocity at inner wall is considered in equations and this time the values of shear stress at both walls should be calculated. If $|\tau_{wo}| < B_c < |\tau_{wi}|$, the inner wall slip regime is dominated but if $|\tau_{wo}| > B_c$, slip occurs at both walls which in this case the values of ψ and $\overline{R}_m$ should be calculated with including both slip velocities in Eqs. (29a) and (31a).

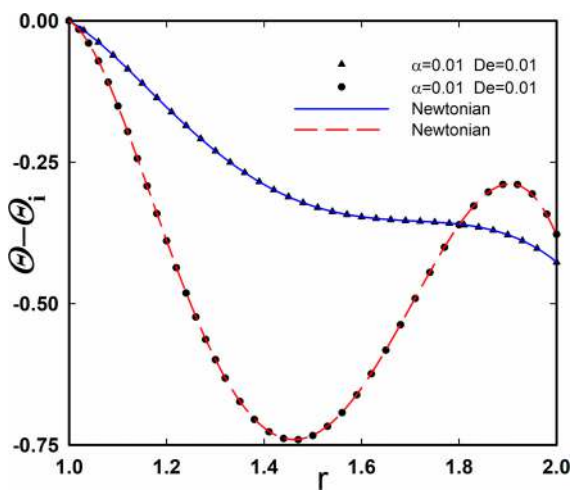

Fig. 3 Dimensionless temperature profile: blue line and (▲) symbol—at Br = 2, $B = 1$, $s = 1$, $B_c = 1$, $\varphi = 1$ and slip at both walls and red line and (●) symbol—at Br = 1, $B = 0.5$, $s = 0.5$, $B_c = 5$, $\varphi = 1000$ and slip just at inner wall

Table 1 Comparison between the obtained Nusselt number value from this study and Pinho and Coelho study [38]

	Newt (no slip) [38]	Newt (B = 10,000)	$\alpha = 0.01$ De = 0.01 (B = 10,000)
Nu_i ($\varphi = 1$)	1.17229	1.17279	1.17270
Nu_o ($\varphi = 1$)	1.07233	1.07572	1.07585
Nu_o ($\varphi = 1000$)	1.39547	1.39930	1.39945
Nu_i ($\varphi = 0.001$)	2.37452	2.37520	2.37508

4.1 Validation. Since the Newtonian fluid has a simple rheological model, the hydrodynamics and heat transfer equations which derived for it can be followed easily. Due to the fact that by putting α and De in the Giesekus equation to zero, the model simplifies to the Newtonian; thus, it is anticipating that if the values of α and De become insignificant, the results achieved for viscoelastic fluid tend to those of Newtonian fluid. By this way, we can validate the Newtonian limit of the derived equations for complex fluids.

The shear rate equation for Newtonian fluid is derived as follows:

$$\overline{\gamma}_{rz} = \frac{d\overline{u}}{d\overline{r}} = \overline{\tau}_{rz} = \frac{\psi \overline{R}_m}{2} \quad \frac{\overline{r}}{\overline{R}_m} - \frac{\overline{R}_m}{\overline{r}} \Bigg) \tag{38}$$

By integrating from Eq. (38) and substituting the boundary conditions, velocity profile will be derived as follows:

$$\overline{u} = \overline{V}|_{\overline{R}_i}^{\overline{r}} + \overline{\mathbf{u}}_{wi} = \frac{\psi}{4}\left(r^2 - R_i^2\right) - \frac{\psi}{2} R_m^2 \ln\left(\frac{r}{R_i}\right) + \overline{\mathbf{u}}_{wi} \tag{39}$$

$\overline{u}_{wi}$ is presented in Eq. (28).

By substituting Eq. (39) in Eq. (17) and twice integrating, the dimensionless heat profile can be obtained as follows:

$$\Theta = X\psi r^2 \left(\frac{r^2}{64} - \frac{R_i^2}{16} + \frac{R_m^2}{8}\left(1 - \ln\left(\frac{r}{R_i}\right)\right)\right) - Br\psi^2\left(\frac{r^4}{64} - \frac{r^2 R_m^2}{8} + \frac{R_m^4}{8}\ln^2(r)\right) + C_1 \ln(r) + C_2 + \frac{\overline{\mathbf{u}}_{wi} r^2}{4} \tag{40}$$

$$X = 1 - \frac{2Br\psi^2}{8\left(R_i^2 - R_o^2\right)}\left(\left(R_i^2 - R_o^2\right)\left(R_i^2 - 4R_m^2 + R_o^2\right) + 4R_m^4 \ln\left(\frac{R_i}{R_o}\right)\right) \tag{41}$$

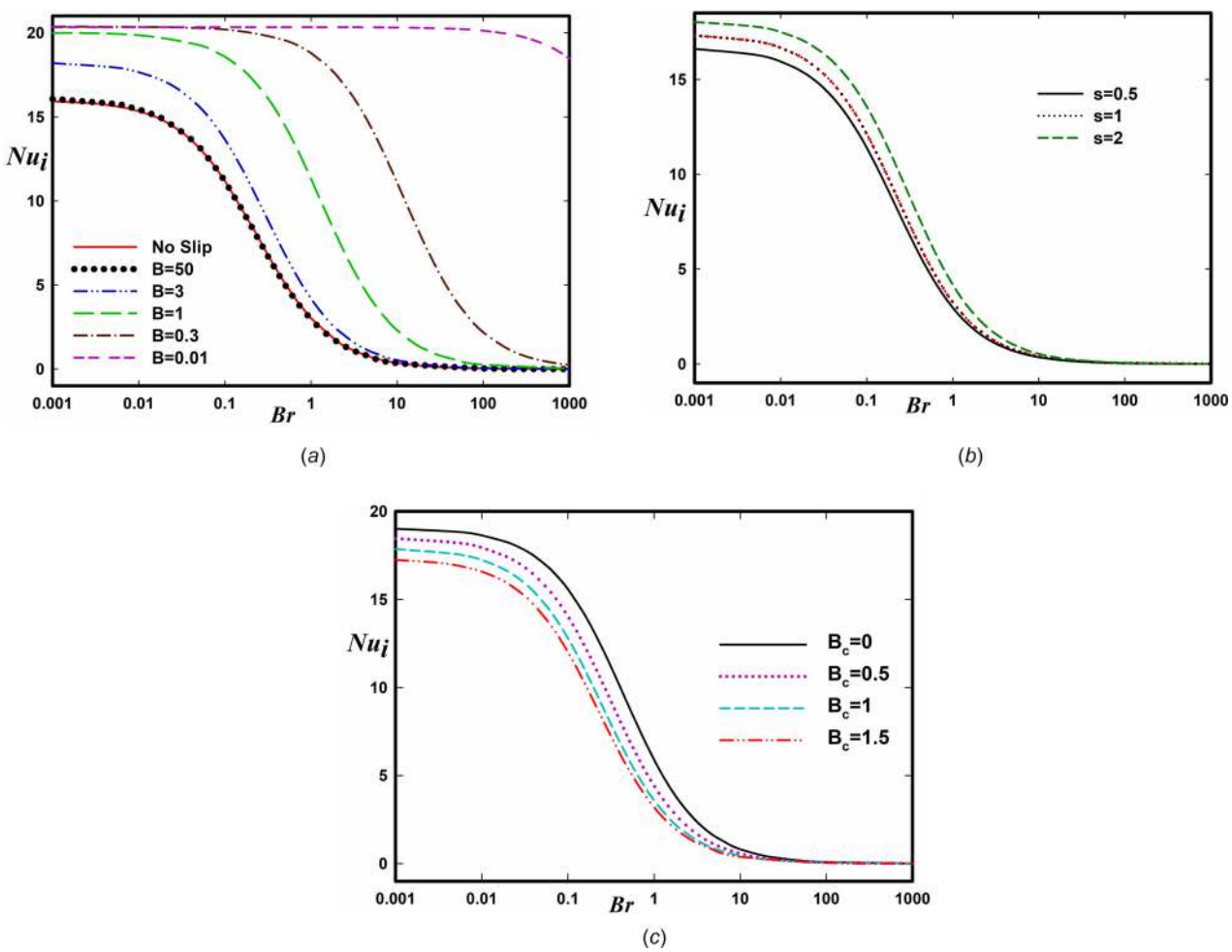

Fig. 4 Variation of Nu_i versus Br and (*a*) dimensionless slip number (*B*) at $s = 1$ and $B_c = 0$ (*b*) power law index of slip (*s*) at $B = 5$ and $B_c = 0$ (*c*) dimensionless slip critical shear stress number (B_c) at $B = 2$ and $s = 1$ in the case of slip at both walls for $\alpha = 0.1$, De = 1, and $\phi = 1$

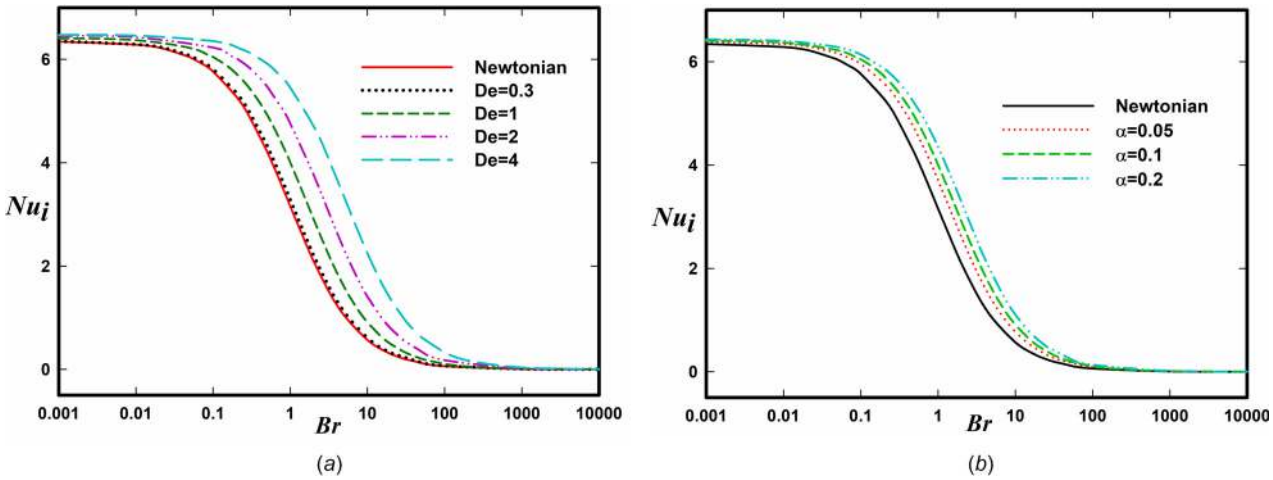

Fig. 5 Variation of Nu_i versus Br and (*a*) Deborah number (De) and $\alpha = 0.1$ (*b*) mobility parameter (α) and De = 1 in the case of slip at both walls for $B = 10$, $s = 1$, $B_c = 0$, and $\varphi = 0.001$

As can be seen from Fig. 3 and Table 1, a very good agreement has been found between the results of Newtonian fluid and viscoelastic model with small value of elasticity which confirm the accuracy of obtained equations for the Giesekus model employed in this study.

4.2 Slip at Both Walls. Since the $B_c = 0$ is always lower than the shear stress at both walls therefore, in this study $B_c = 0$ is investigated. That corresponds to slip at both walls. Figure 4(*a*) shows the effects of the Brinkman number and dimensionless slip numbers on the inner wall Nusselt number for $\varphi = 1$. It is seen that the

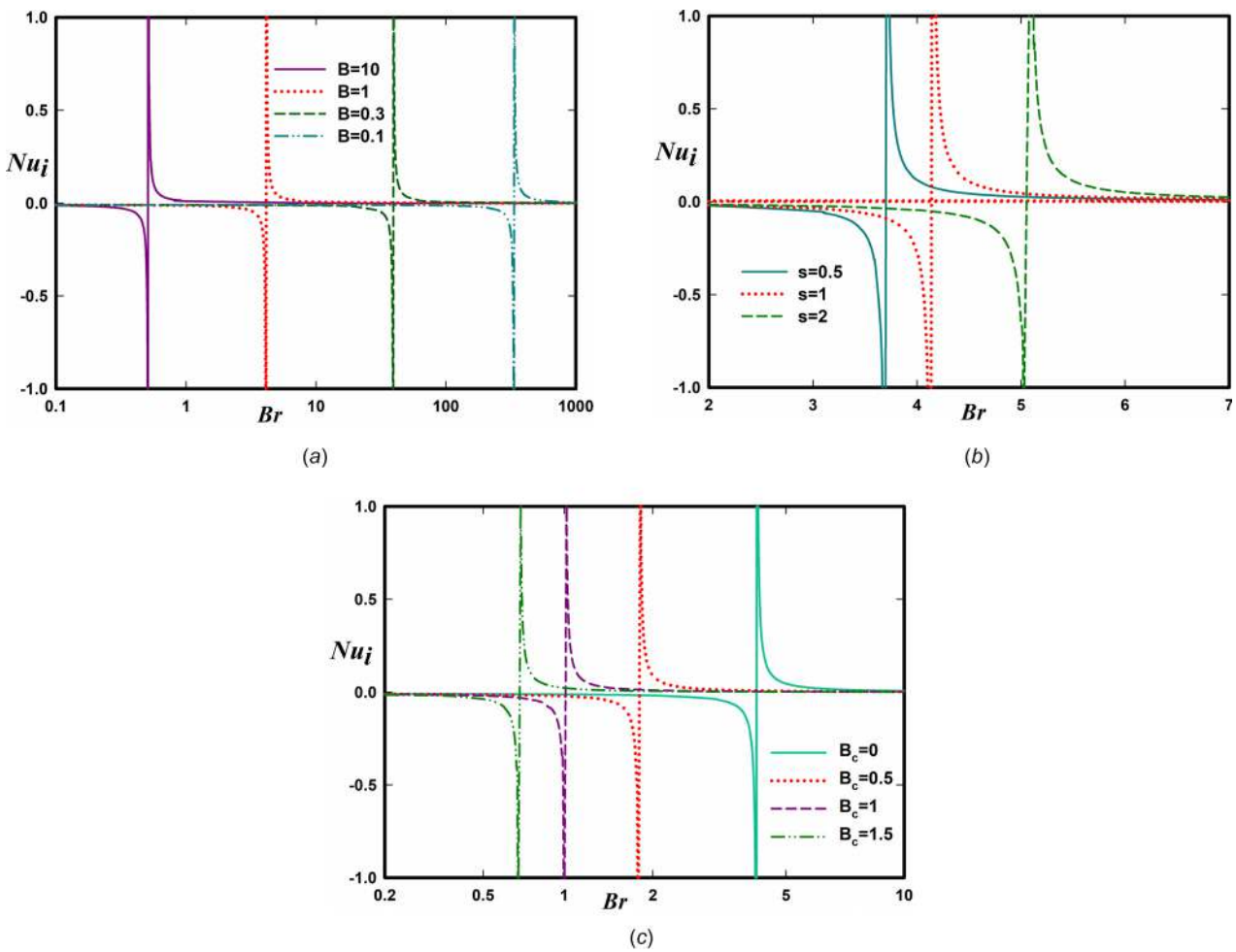

Fig. 6 Variation of Nu_i versus Br and (*a*) dimensionless slip number (B) at $s = 1$ and $B_c = 0$ (*b*) power law index of slip (s) at $B = 1$ and $B_c = 0$ (*c*) dimensionless slip critical shear stress number (B_c) at $B = 1$ and $s = 1$ in the case of slip at both walls for $\alpha = 0.1$, De = 1, and $\varphi = 1000$

Nusselt number decreases by raising the Brinkman number because the heat generation by viscous dissipation increases in that case. This behavior is stronger near the walls and is expected because, according to the viscous dissipation function (Eq. (8)), both shear stress and velocity gradient attain their maximum values adjacent to the walls [7]. Therefore, the difference between wall temperature and bulk temperature increases, and as a result, the Nusselt number decreases. Also, the effect of slip on the Nusselt number is noticeable, so that by increasing the slip effect (decreasing slip number) the Nusselt number increases. Indeed, by decreasing slip number both shear stress and velocity gradient decrease and therefore viscous dissipation is reduced, thereby Nusselt number increases.

Figures 4(*b*) and 4(*c*) present the influence of power law index of slip (s) and dimensionless slip critical shear stress number (B_c) on the inner wall Nusselt number at $\varphi = 1$. Slip critical shear stress numbers are chosen such that the slip always occurs at both walls. As increasing s and decreasing B_c cause an increase in wall slip velocity, the behavior of Nusselt number by increasing s and decreasing B_c is similar to the one when decreasing slip number. The effect of elasticity (α, De) on Nusselt number is shown in Fig. 5 for the case of $\varphi = 0.001$. Increasing the elasticity due to shear-thinning behavior of the fluid decreases the internal heat produced by viscous dissipation and therefore causes the enhancement of Nusselt number.

The trend for inner Nusselt number is different for $\varphi = 1000$, as indicated in Fig. 6. The Nusselt number is negative for low Brinkman numbers. By increasing the Brinkman number, a singularity appears in the Nusselt curve which is called critical Brinkman number and finally becomes positive for high Brinkman numbers. In the case of $\varphi = 1000$ because of insulating circumstances at the inner wall, the wall temperature is lower than the bulk temperature and according to the dimensionless temperature and Nusselt number expressions, Nusselt becomes negative. As by increasing the Brinkman number due to the higher heat generation near the wall, the difference between the bulk temperature and the wall temperature reduces, and at a critical Brinkman number, this difference vanishes. As a result, the Nusselt number diverges. If the Brinkman number increases even more, the inner wall temperature will be higher than the bulk temperature and then the Nusselt becomes positive.

Increasing slip effect by increasing s or decreasing B and B_c due to the reduction of the heat generation by viscous dissipation increases the critical Brinkman number. In other words, the singularity in Nusselt curve occurs at higher Brinkman number because by decreasing viscous dissipation, the reduction of the difference between the bulk temperature and the wall temperature will be slower.

4.3 Slip Only at the Inner Wall. The shear stress for $B_c = 2.2$ and $\alpha = 0.1$, $De = 1$ is always lower than $|\tau_{wi}|$ and higher than $|\tau_{wo}|$ and slip occurs only at the inner wall for any value of B and s.

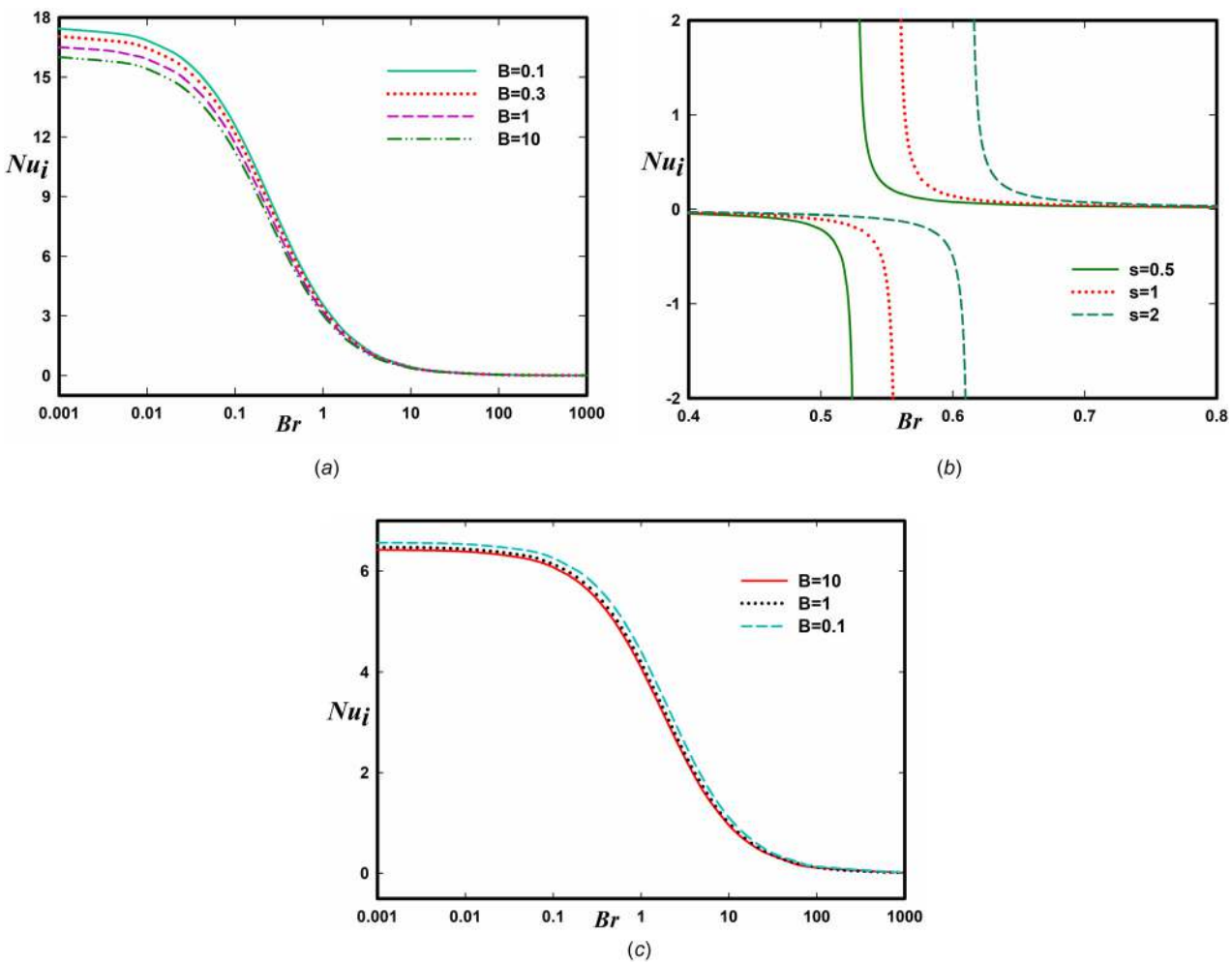

Fig. 7 Variation of Nu_i versus Br and (*a*) dimensionless slip number (B) at $s = 1$, $B_c = 2.2$ and $\varphi = 1$ (*b*) power law index of slip (s) at $B = 1$, $B_c = 2.2$ and $\varphi = 1000$ (*c*) dimensionless slip number (B) at $s = 1$, $B_c = 2.2$, and $\varphi = 0.001$ in the case of slip only at inner wall for $\alpha = 0.1$ and De = 1

Therefore, in this study $B_c = 2.2$ is considered. This corresponds to a regime where the slip occurs only at the inner wall. Figure 7 shows the effect of B and s on the inner wall Nusselt number.

It can be shown that the shape of the Nusselt curve is almost similar to the case of slip at both walls. However, we can notice a difference between the two former cases: in the case of slip only at the inner wall the variation of Nusselt number with slip parameters is weaker because the plug flow never occurs. It means that the pressure gradient and the shear stress will not reduce significantly by wide decrease in B or increasing s; therefore, the effect of slip parameters on the viscous dissipation in the case of slip only at the inner wall is weaker than when slip occurs at both walls. As a result, the thermal behavior of the fluid is less affected by the viscous dissipation effects. Because of the weak effect of slip parameters on viscous dissipation function, the critical Brinkman number will be lower than the one in situation of slip at both walls. With a comparison between the Nusselt profiles for $\varphi = 0.001$ and $\varphi = 1$, it can be understood that the Nusselt number for $\varphi = 0.001$ is lower than $\varphi = 1$. In the case of $\varphi = 0.001$, because the heat flux dominates at the inner wall, which causes be higher wall temperature and according to Eq. (37a), inner wall Nusselt number for $\varphi = 0.001$ is lower than inner wall Nusselt number for $\varphi = 1$. Figure 8 shows the effects of slip parameters and Brinkman number on dimensionless temperature distribution at three selected φ values. It can be seen from Fig. 8(a) that for the negligible viscous dissipation, the process of fluid temperature increasing occurs uniformly from colder wall to the warmer wall but by increasing Brinkman number the temperature profile shows a maximum. As explained before, this behavior is due to the stronger effect of viscous dissipation near the walls which increases the temperature difference the wall and the fluid by increasing Brinkman number. Therefore, a maximum point appears in the temperature profile. The effect of slip parameters on the temperature profile is the opposite than the effect of the Brinkman number. Indeed, by increasing the slip effect, the internal heat generation by viscous dissipation is reduced, and therefore, the

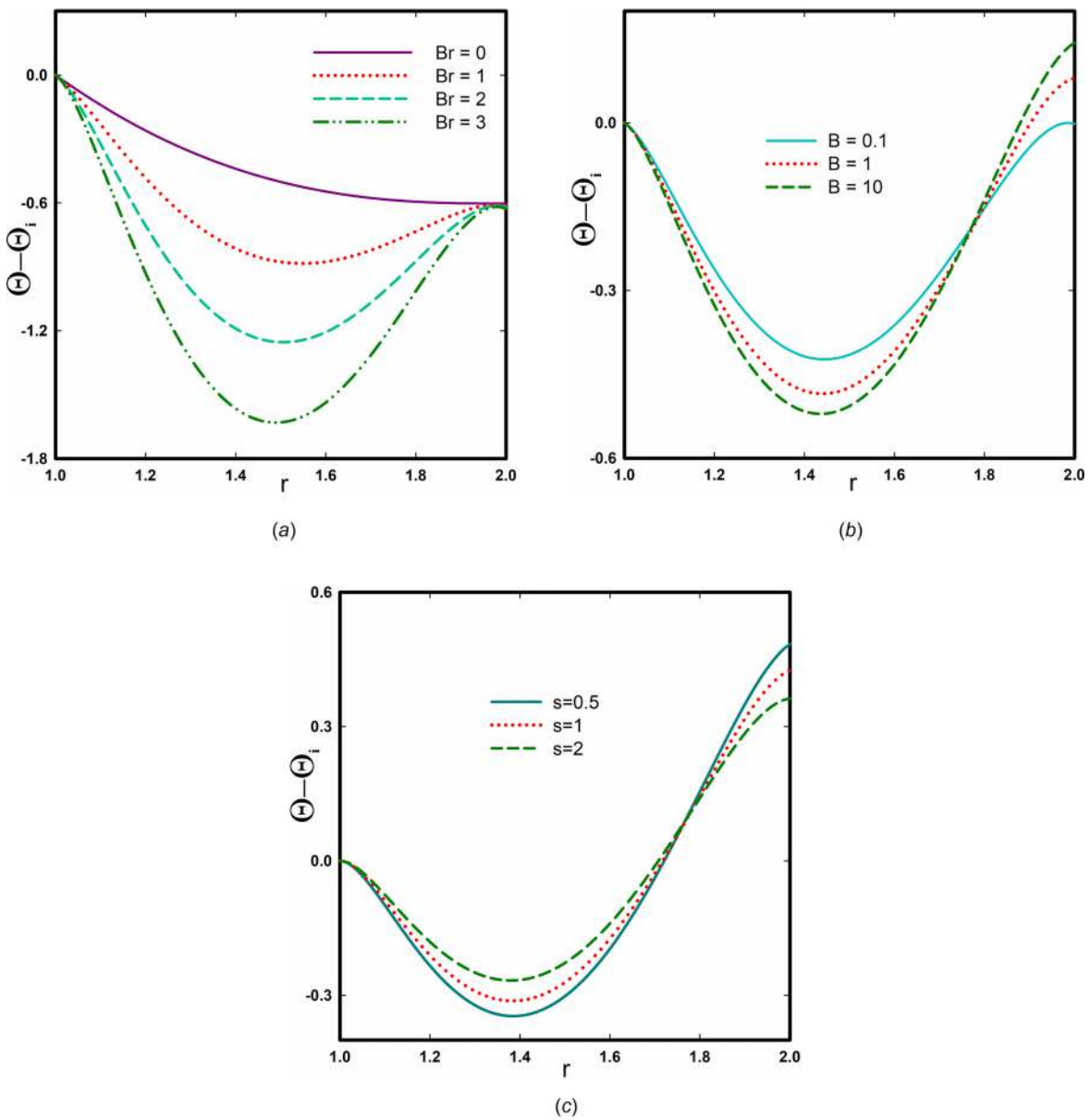

Fig. 8 Dimensionless temperature profile with variation of (*a*) Brinkman number (Br) at $B = 1$, $s = 1$, $B_c = 2.2$, and $\varphi = 0.001$ (*b*) dimensionless slip number (B) at Br = 1, $B = 1$, $B_c = 2.2$, and $\varphi = 1$ (*c*) power law index of slip (s) at Br = 1, $B = 1$, $B_c = 2.2$, and $\varphi = 1000$ in the case of slip only at inner wall for $\alpha = 0.1$, De = 1

difference between the wall temperature and the fluid temperature decreases.

5 Conclusion

Forced convection heat transfer for viscoelastic fluid obeying Giesekus model is investigated analytically in coaxial microannulus geometry under steady, laminar, thermal, and hydrodynamical fully developed conditions. The nonlinear Navier slip law was employed at both walls when the wall shear stresses reach a critical value which is known as the slip critical shear stress. Since the shear stress at inner walls is always higher than the one at the outer wall, there are two possible slip flow regimes, namely slip only at the inner wall and slip at both walls. Thermal boundary conditions were peripherally and axially constant heat flux. Various inner–outer wall heat flux ratios were analyzed in the study. The effects of slip parameters (B, B_c, s), elasticity (α, De), and viscous dissipation (Br) on the Nusselt number and the temperature profile were investigated. Results for heat flux dominant at the inner wall ($\varphi = 0.001$) and same heat flux at both walls ($\varphi = 1$) highlight that increasing the slip effect and the elasticity or decreasing the Brinkman number tends to increase the Nusselt number. But in the case of a heat flux dominant at the outer wall ($\varphi = 1000$), the Nusselt curve shows a singularity at a critical Brinkman number because the wall temperature will be equal to the bulk temperature by internal viscous dissipation. Increasing the slip effect delays this critical Brinkman number by reducing the shear stresses and shear rates.

Appendix

This appendix details the expressions of the coefficients presented along the paper.
The hydrodynamic solution coefficients are

$$P_1 = De^2\alpha\psi^2, \quad P_2 = 1+\overline{R}_m^2 De^2\alpha\psi^2, \quad P_3 = 1-2\alpha+\overline{R}_m^2 P_1\,(2-3\alpha), \quad P_4 = P_1^2\overline{R}_m^4 - (1+P_2)\,(1+3P_2),$$
$$P_5 = 4P_1^2\overline{R}_m^4 - 4(1+P_2)^2, \quad P_6 = 2\sqrt{P_2} - 2 - P_1\overline{R}_m^2, \quad P_7 = 2\sqrt{P_2} + 2 + P_1\overline{R}_m^2$$

In this appendix, we expand the expression of X, Φ^*, and U^* introduced in Eqs. (18a), (33a), and (33b), respectively. After development, we obtain

$$X = 1+\frac{2\,Br}{\overline{R}_o^2-\overline{R}_i^2}\quad P_{33}\left(\overline{R}_o^2-\overline{R}_i^2\right)+\frac{\psi^2}{P_1^2}\frac{P_{39}+P_{40}\overline{R}_o^2}{P_2H^2\,P_{43}}-\frac{\psi^2}{P_1^2}\frac{P_{39}+P_{40}\overline{R}_o^2}{P_2H^2\,P_{44}}$$
$$+0.5\,P_{41}\ln\left(\frac{P_8-P_1\overline{R}_o^2}{P_8-P_1\overline{R}_i^2}\right)-0.5\,P_{42}\ln\quad\frac{P_9+P_1\overline{R}_o^2}{P_9+P_1\overline{R}_i^2}\Bigg)\Bigg)$$

$$\Phi^* = 0.5\left(\begin{array}{l} P_{33}\,\overline{r}^2 - P_{34}\ln(\overline{r}) + P_{35}\ln\left(P_{37}-P_1\,\overline{r}^2\right) + P_{36}\ln\left(P_{38}+P_1\,\overline{r}^2\right) + P_{42}\begin{pmatrix}\ln(P_8)\ \ln(\overline{r})\\ -0.5\ Li_2\quad\left[\dfrac{P_1\,\overline{r}^2}{P_8}\right]\end{pmatrix} \\ -P_{43}\left(\ln(P_9)\ \ln(\overline{r}) - 0.5\ Li_2\quad\left[-\dfrac{P_1\,\overline{r}^2}{P_9}\right]\right)\end{array}\right)$$

$$U^* = -\frac{\psi}{8}\left(\begin{array}{l} P_{24}\,\overline{r}^2 + P_{26}\ln(\overline{r}) + P_{25}\ln\left(P_8-P_1\,\overline{r}^2\right) + \dfrac{P_{19}P_9\ln\left(P_9+P_1\,\overline{r}^2\right)}{2P_1} \\ +\overline{r}^2\left(0.5\,P_{11}\ln\quad\dfrac{P_9+P_1\,\overline{r}^2}{P_8-P_1\,\overline{r}^2}\right)+P_{27}\ln\quad\dfrac{P_8-P_1\,\overline{r}^2}{P_8-P_1\,\overline{R}_i^2}\Bigg)\Bigg) \\ -0.5\left(P_{13}\,Li_2\left[\dfrac{P_1\,\overline{r}^2}{P_8}\right]+P_{14}Li_2\left[-\dfrac{P_1\,\overline{r}^2}{P_9}\right]\right)+P_{28}\ln\quad\dfrac{P_9+P_1\,\overline{r}^2}{P_9+P_1\,\overline{R}_i^2}\Bigg) \\ -0.5\left(P_{13}\,Li_2\left[\dfrac{P_1\,\overline{r}^2}{P_8}\right]+P_{14}Li_2\left[-\dfrac{P_1\,\overline{r}^2}{P_9}\right]\right)\end{array}\right)+\frac{1}{4}\,\overline{\boldsymbol{u}}_{\boldsymbol{wi}}\left(\overline{r}^2-\overline{R}_i^2\right)$$

with the following subexpressions:

$$P_8 = 1+P_2+2\sqrt{P_2},\;\; P_9 = -1-P_2+2\sqrt{P_2},\;\; P_{10} = 1+2P_2-P_2^2,\;\; P_{11} = \frac{\overline{R}_m^2+\overline{R}_m^4 P_1\,(2\alpha-1)}{P_2\sqrt{P_2}},$$

$$P_{12} = \frac{(2\alpha-1)}{P_1\sqrt{P_2}},\;\; P_{13} = -\frac{P_8\,(P_{12}\,P_8-P_{11})}{P_1},\;\; P_{14} = \frac{P_9\,(P_{12}\,P_9+P_{11})}{P_1},$$

$$P_{15} = \sqrt{1+(1+3P_2)^2+4P_2-4P_2^3+P_2^4-2(1+3P_2)P_{10}+2P_2^2-P_2^2\overline{R}_m^4P_1^2},\;\; P_{16} = -P_2-{P_2}^2,$$

$$P_{17} = -\frac{4\left((1+3P_2)^2-P_1^2\overline{R}_m^4P_2+(1+3P_2)(-P_{10}+P_{15})\right)(\alpha-1)}{P_2P_1^2P_{15}},\;\; P_{18} = \frac{4\left((1+3P_2)^2-\overline{R}_m^4P_1^2P_2-(1+3P_2)(P_{10}+P_{15})\right)(\alpha-1)}{P_2P_1^2P_{15}},$$

$$P_{19} = P_{11}+P_{12}\,P_9,\;\; P_{20} = -P_{11}+P_{12}\,P_8,\;\; P_{21} = P_1\left(\overline{R}_m^4P_1P_2+\overline{R}_i^2\left(2-2(1+3P_2)+4P_2-2P_2^2+P_2P_1\overline{R}_i^2\right)\right),$$

$$P_{22} = 8\,(1-\alpha)\left((1+3P_2)\overline{R}_i^2-\overline{R}_m^4P_1\right)+8P_1P_{12}\overline{R}_i^2\sqrt{P_2}P_{16}+4P_2\sqrt{P_2}P_1^2P_{12}\left(\overline{R}_m^4+\overline{R}_i^4\right),$$

$$P_{23} = \overline{R}_m^4P_1^2P_2P_{11}+2P_1P_{11}\overline{R}_i^2\,P_{16}+P_1^2P_{11}\overline{R}_i^4P_2,\;\; P_{24} = 0.5\left(P_{11}-P_{19}-\frac{P_{23}}{P_{21}}-\frac{P_{22}}{P_{21}}-P_{20}-\frac{P_{23}}{P_{21}}\ln\;\frac{P_9+P_1\overline{R}_i^2}{P_8-P_1\overline{R}_i^2}\right)\right),$$

$$P_{25} = \frac{0.5P_8}{P_1}\left(P_{11}-\frac{P_{23}}{P_{21}}-P_{20}\right),\;\; P_{26} = P_{13}\ln|P_8|+P_{14}\ln|P_9|+P_{17}\ln|P_{15}-P_{16}|+P_{18}\ln|P_{15}+P_{16}|,$$

$$P_{27} = 0.5\left(\frac{P_{23}}{P_{21}}+P_{20}\right),\;\; P_{28} = 0.5\,(P_{19}-P_{11}),\;\; P_{29} = 1+{P_2}^2-\overline{R}_m^4P_1^2,\;\; P_{30} = \sqrt{1+2P_2+{P_2}^2-\overline{R}_m^4P_1^2},$$

$$P_{31} = \frac{\overline{R}_m^4\,(\alpha-1)\,\psi^2}{P_2\sqrt{P_2}},\;\; P_{32} = \frac{\psi^2(4\alpha-3)}{P_1^2\sqrt{P_2}},\;\; P_{33} = \frac{1-2\alpha}{2\alpha De^2},\;\; P_{34} = \frac{4\psi^2\,(1+P_2)\,(\alpha-1)}{P_2P_1^2},\;\; P_{35} = \frac{(P_{30}-P_{29}+P_2(6+P_{30}))\,\psi^2\,(\alpha-1)}{P_2P_1^2P_{30}}$$

$$P_{36} = \frac{(P_{30}+P_{29}+P_2(-6+P_{30}))\,\psi^2\,(\alpha-1)}{P_2P_1^2P_{30}},\;\; P_{37} = 1+P_2+P_{30},\;\; P_{38} = -1-P_2+P_{30},\;\; P_{39} = -4\overline{R}_m^4P_1\,(1+P_2)\,(\alpha-1),$$

$$P_{40} = 4\left(8P_2+\overline{R}_m^4P_1^2\right)(\alpha-1),\;\; P_{41} = P_{31}-P_8P_{32},$$

$$P_{42} = P_{31}+P_9P_{32},\;\; P_{43} = \overline{R}_m^4P_1-2\,(1+P_2)\overline{R}_o^2+\overline{R}_o^4P_1,\;\; P_{44} = \overline{R}_m^4P_1-2\,(1+P_2)\overline{R}_i^2+\overline{R}_i^4P_1$$

$\mathrm{Li}_n(z)$ is the polylogarithm function defined by

$$\mathrm{Li}_n(z) = \sum_{k=1}^{\infty}\frac{z^k}{k^n}$$

References

[1] Tian, W.-C., and Finehout, E., 2008, "Introduction to Microfluidics," *Microfluidics for Biological Applications*, Springer, Boston, MA, pp. 1–34.

[2] Karniadakis, G., Beskok, A., and Aluru, N., 2006, *Microflows and Nanoflows: Fundamentals and Simulation*, Springer Science & Business Media, New York.

[3] Volpatti, L. R., and Yetisen, A. K., 2014, "Commercialization of Microfluidic Devices," Trends Biotechnol., **32**(7), pp. 347–350.

[4] Whitesides, G. M., 2006, "The Origins and the Future of Microfluidics," Nature, **442**(7101), pp. 368–373.

[5] Ghallab, Y., and Badawy, W., 2004, "Sensing Methods for Dielectrophoresis Phenomenon: From Bulky Instruments to Lab-on-a-Chip," IEEE Circuits Syst. Mag., **4**(3), pp. 5–15.

[6] Denn, M. M., 2001, "Extrusion Instabilities and Wall Slip," Annu. Rev. Fluid Mech., **33**(1), pp. 265–287.

[7] Mohseni, M. M., and Rashidi, F., 2015, "Axial Annular Flow of a Giesekus Fluid With Wall Slip Above the Critical Shear Stress," J. Non-Newtonian Fluid Mech., **223**, pp. 20–27.

[8] Damianou, Y., Philippou, M., Kaoullas, G., and Georgiou, G. C., 2014, "Cessation of Viscoplastic Poiseuille Flow With Wall Slip," J. Non-Newtonian Fluid Mech., **203**, pp. 24–37.

[9] Chatzimina, M., Georgiou, G. C., Housiadas, K., and Hatzikiriakos, S. G., 2009, "Stability of the Annular Poiseuille Flow of a Newtonian Liquid With Slip Along the Walls," J. Non-Newtonian Fluid Mech., **159**(1–3), pp. 1–9.

[10] Ferrás, L., Nóbrega, J., and Pinho, F., 2012, "Analytical Solutions for Newtonian and Inelastic Non-Newtonian Flows With Wall Slip," J. Non-Newtonian Fluid Mech., **175**, pp. 76–88.

[11] Ferrás, L. L., Nóbrega, J. M., and Pinho, F. T., 2012, "Analytical Solutions for Channel Flows of Phan–Thien–Tanner and Giesekus Fluids Under Slip," J. Non-Newtonian Fluid Mech., **171**, pp. 97–105.

[12] Kalyon, D. M., and Malik, M., 2012, "Axial Laminar Flow of Viscoplastic Fluids in a Concentric Annulus Subject to Wall Slip," Rheol. Acta, **51**(9), pp. 805–820.

[13] Matthews, M., and Hill, J., 2007, "Newtonian Flow With Nonlinear Navier Boundary Condition," Acta Mech., **191**(3–4), pp. 195–217.

[14] Kaoullas, G., and Georgiou, G. C., 2013, "Newtonian Poiseuille Flows With Slip and Non-Zero Slip Yield Stress," J. Non-Newtonian Fluid Mech., **197**, pp. 24–30.

[15] Housiadas, K. D., 2013, "Viscoelastic Poiseuille Flows With Total Normal Stress Dependent, Nonlinear Navier Slip at the Wall," Phys. Fluids, **25**(4), p. 043105.

[16] Tang, H., and Kalyon, D. M., 2008, "Unsteady Circular Tube Flow of Compressible Polymeric Liquids Subject to Pressure-Dependent Wall Slip," J. Rheol., **52**(2), pp. 507–525.

[17] Tang, H., and Kalyon, D. M., 2008, "Time-Dependent Tube Flow of Compressible Suspensions Subject to Pressure Dependent Wall Slip: Ramifications on Development of Flow Instabilities," J. Rheol., **52**(5), pp. 1069–1090.

[18] Pereira, G., 2009, "Effect of Variable Slip Boundary Conditions on Flows of Pressure Driven Non-Newtonian Fluids," J. Non-Newtonian Fluid Mech., **157**(3), pp. 197–206.

[19] Damianou, Y., Georgiou, G. C., and Moulitsas, I., 2013, "Combined Effects of Compressibility and Slip in Flows of a Herschel–Bulkley Fluid," J. Non-Newtonian Fluid Mech., **193**, pp. 89–102.

[20] Barkhordari, M., and Etemad, S. G., 2007, "Numerical Study of Slip Flow Heat Transfer of Non-Newtonian Fluids in Circular Microchannels," Int. J. Heat Fluid Flow, **28**(5), pp. 1027–1033.

[21] Ngoma, G. D., and Erchiqui, F., 2007, "Heat Flux and Slip Effects on Liquid Flow in a Microchannel," Int. J. Therm. Sci., **46**(11), pp. 1076–1083.

[22] Shojaeian, M., and Koşar, A., 2014, "Convective Heat Transfer and Entropy Generation Analysis on Newtonian and Non-Newtonian Fluid Flows Between Parallel-Plates Under Slip Boundary Conditions," Int. J. Heat Mass Transfer, **70**, pp. 664–673.

[23] Anand, V., 2014, "Slip Law Effects on Heat Transfer and Entropy Generation of Pressure Driven Flow of a Power Law Fluid in a Microchannel Under Uniform Heat Flux Boundary Condition," Energy, **76**, pp. 716–732.

[24] Kiyasatfar, M., 2018, "Convective Heat Transfer and Entropy Generation Analysis of Non-Newtonian Power-Law Fluid Flows in Parallel-Plate and Circular Microchannels Under Slip Boundary Conditions," Int. J. Therm. Sci., **128**, pp. 15–27.

[25] Mohseni, M. M., Tissot, G., and Badawi, M., 2018, "Forced Convection Heat Transfer of Giesekus Fluid With Wall Slip Above the Critical Shear Stress in Pipes," Int. J. Heat Fluid Flow, **71**, pp. 442–450.

[26] Kakac, S., Yener, Y., and Pramuanjaroenkij, A., 2013, *Convective Heat Transfer*, CRC Press, Boca Raton, FL.

[27] Pinho, F., and Oliveira, P., 2000, "Analysis of Forced Convection in Pipes and Channels With the Simplified Phan-Thien–Tanner Fluid," Int. J. Heat Mass Transfer, **43**(13), pp. 2273–2287.
[28] Bird, R. B., Armstrong, R. C., and Hassager, O., 1987, *Dynamics of Polymeric Liquids* (Fluid Mechanics), Vol. 1, Wiley, New York.
[29] Mohseni, M. M., Rashidi, F., and Movagar, M. R. K., 2015, "Analysis of Forced Convection Heat Transfer for Axial Annular Flow of Giesekus Viscoelastic Fluid," Korean Chem. Eng. Res., **53**(1), pp. 91–102.
[30] Giesekus, H., 1983, "Stressing Behaviour in Simple Shear Flow as Predicted by a New Constitutive Model for Polymer Fluids," J. Non-Newtonian Fluid Mech., **12**(3), pp. 367–374.
[31] Giesekus, H., 1982, "A Simple Constitutive Equation for Polymer Fluids Based on the Concept of Deformation-Dependent Tensorial Mobility," J. Non-Newtonian Fluid Mech., **11**(1–2), pp. 69–109.
[32] Bird, R., Stewart, W. E., and Lightfoot, E. N., 2002, *Transport Phenomena*, 2nd ed., Wiley, London.
[33] Bejan, A., 2013, *Convection Heat Transfer*, Wiley, Hoboken, NJ.
[34] Yoo, J., and Choi, H. C., 1989, "On the Steady Simple Shear Flows of the One-Mode Giesekus Fluid," Rheol. Acta, **28**(1), pp. 13–24.
[35] Schleiniger, G., and Weinacht, R. J., 1991, "Steady Poiseuille Flows for a Giesekus Fluid," J. Non-Newtonian Fluid Mech., **40**(1), pp. 79–102.
[36] Mohseni, M. M., and Rashidi, F., 2010, "Viscoelastic Fluid Behavior in Annulus Using Giesekus Model," J. Non-Newtonian Fluid Mech., **165**(21–22), pp. 1550–1553.
[37] Jouyandeh, M., Mohseni, M. M., and Rashidi, F., 2017, "Tangential Flow Analysis of Giesekus Model in Concentric Annulus With Both Cylinders Rotation," J. Appl. Fluid Mech., **10**(6), pp. 1–9.
[38] Coelho, P., and Pinho, F., 2006, "Fully-Developed Heat Transfer in Annuli With Viscous Dissipation," Int. J. Heat Mass Transfer, **49**(19–20), pp. 3349–3359.